Since January 2020 Elsevier has created a COVID-19 resource centre with free information in English and Mandarin on the novel coronavirus COVID-19. The COVID-19 resource centre is hosted on Elsevier Connect, the company's public news and information website.

Elsevier hereby grants permission to make all its COVID-19-related research that is available on the COVID-19 resource centre - including this research content - immediately available in PubMed Central and other publicly funded repositories, such as the WHO COVID database with rights for unrestricted research re-use and analyses in any form or by any means with acknowledgement of the original source. These permissions are granted for free by Elsevier for as long as the COVID-19 resource centre remains active.

Analytica Chimica Acta 1234 (2022) 340523

Contents lists available at ScienceDirect

Analytica Chimica Acta

journal homepage: www.elsevier.com/locate/aca

One-click investigation of shape influence of silver nanostructures on SERS performance for sensitive detection of COVID-19

Zehua Li [b,1], Yong Luo [a,b,1], Yongchao Song [c,1], Qinglin Zhu [b], Tailin Xu [a,b,*], Xueji Zhang [a]

[a] School of Biomedical Engineering, Health Science Center, Shenzhen University, Shenzhen, Guangdong, 518060, PR China
[b] Research Center for Bioengineering and Sensing Technology, University of Science and Technology Beijing, Beijing, 100083, PR China
[c] Research Center for Intelligent and Wearable Technology, College of Textiles and Clothing, State Key Laboratory of Bio-Fibers and Eco-Textiles, Qingdao University, Qingdao, 266071, PR China

HIGHLIGHTS

- Multiple parameters can be adjusted by one-click on the integrated electrochemical array.
- Various morphologies can be synthesized for screening the SERS performance.
- The platform can achieve high-throughput and simultaneous SERS sensing.

GRAPHICAL ABSTRACT

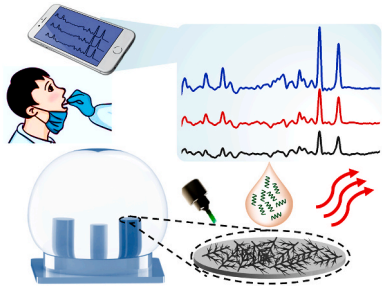

ARTICLE INFO

Keywords:
SERS
Ag nanostructure
Mini-pillar platform
COVID-19
Microdroplets array

ABSTRACT

Sensitive and accurate detection of SARS-CoV-2 methods is meaningful for preventing and controlling the novel coronavirus. The detection techniques supporting portable, onsite, in-time, and online data transfer are urgently needed. Here, we one-click investigated the shape influence of silver nanostructures on SERS performance and their applications in the sensitive detection of SARS-CoV-2. Such investigation is achieved by adjusting multiple parameters (concentration, potential, and time) on the integrated electrochemical array, thus various morphologies (e.g., bulk, dendritic, globular, and spiky) can be one-click synthesized. The SERS performance results indicated that dendritic nanostructures are superior to the other three with an order of magnitude signal enhancement. Such on-electrode dendritic silver substrate also represents high sensitivity (LOD = 7.42×10^{-14} M) and high reproducibility (RSD = 3.67%) toward the SARS-CoV-2 RNA sequence detection. Such approach provides great potentials for rapid diagnosis and prevention of diverse infectious diseases.

1. Introduction

Since December 2019, the novel coronavirus pneumonia (COVID-19) as a new severe acute respiratory disease with accompanied by breathing distress, fever, cough, and other symptoms began to spread rapidly worldwide [1–4]. Today, reverse-transcription polymerase

* Corresponding author. School of Biomedical Engineering, Health Science Center, Shenzhen University, Shenzhen, Guangdong, 518060, PR China.
E-mail address: xutailin@szu.edu.cn (T. Xu).
[1] These authors contribute to the paper equally.

https://doi.org/10.1016/j.aca.2022.340523
Received 20 September 2022; Received in revised form 11 October 2022; Accepted 12 October 2022
Available online 18 October 2022
0003-2670/© 2022 Elsevier B.V. All rights reserved.

chain reaction (RT-PCR) is widely used to detect clinical samples, such as nasal, pharyngeal swabs, and blood, known as the "gold standard" technique [5–8]. At present, the main assay techniques include chest computed tomography (CT), Enzyme linked immunosorbent assay (ELISA), chemiluminescent immunoassay, and Colloidal gold immunoassay, but they generally requires relatively high qualification requirements, relatively long detection time, cumbersome operation steps, and easy contamination [9]. Therefore, it is urgent to develop a rapid, practical, high accuracy and convenient detection system to deal with the soaring novel coronavirus infection in the world.

SERS with the advantage of high sensitivity has been widely used in airport explosion-proof security checks. Most Raman peaks have a narrow width suitable for multiplex analysis, and the measurements can be conveniently made under ambient and aqueous conditions, etc. [10] Recently, handheld SERS has attracted increasing interest in biological analysis [11]. Silver nanomaterials with various nanostructures are widely used for SERS biosensing chips due to their high electrical/thermal conductivities [12–21]. These research work indicated that the SERS property of silver nanomaterials are highly dependent on their size and morphology [22]. However, most of the work is limited to the use of single structure silver nanostructures to construct SERS biosensing chips. The research on the relationship between the morphology and SERS property of silver nanostructures is relatively scarce [23]. Therefore, by adjusting different parameters, the preparation of silver nanostructures with different morphologies and the rapid screening of optimal Raman enhancement performance can be realized [24–26], which is of great significance for constructing an accurate COVID-19 detection platform [27–33].

Here, we one-click synthesized multiple silver nanostructures by integrated electrodeposition platform for sensitive SARS-CoV-2 RNA sequence SERS detection. Such platform can achieve simultaneously detecting multiple biomarkers or repeatedly detecting on the same biomarkers for enhancing the reproducibility. In our experiments, four different silver nanostructures were one-click synthesized by adjusting different electrodeposition parameters, SERS performance results indicated that the dendritic silver nanostructures had better signal enhancement effect comparing with other three silver nanostructures. Such platform has great potential to meet the diverse clinical medicine and disease control needs of the future.

2. Experimental section

2.1. Materials and instruments

Silver nitrate ($AgNO_3$)was purchased from Guangzhou Jinhua Chemical Reagent Co. Ltd. Potassium nitrate (KNO_3) was purchased from Beijing Chemical Plant Co. Ltd. Polydimethylsiloxane (PDMS) was purchased from Dow Europe GmbH. Sulfuric acid (H_2SO_4, 98%, AR), acetone (>99.5%, AR), ethanol (>99.8%, GR), and Rhodamine6G were purchased from Sigma-Aldrich. The template with 4 × 4 array throughholes was custom made from Beijing Zhongjingkeyi Technology Co. Ltd, China. All other reagents were commercially available and of analytical reagent grade. All solutions were prepared with ultrapure water (Milli-Q, 18.2 MU cm). All experiments were carried out at room temperature (25 °C).

Electrochemical deposition of silver nanostructure was carried out by a homemade device connected with a CHI-660D electrochemical workstation (CHI instruments, shanghai, China). The morphologies of dendritic gold nanostructures were observed by Scanning electron microscope (SEM, JSM-6700 F, Japan).

2.2. Sequence information of the capture, target, and detection probe

The oligonucleotides sequences were synthesized from Sangon Biotech (Shanghai, China). The sequences were as follows:

Target SARS-CoV-2 sequence: 5′-ACACCAAAAGAUCACAUUGG-3'.

Capture probe: 5′-CTTTTGGTGTAAAAAAAAAA-SH C6-3'.

Detection probe: 5′-ROX-AAAAAAAAAACCAATGTGAT-3'.

2.3. Fabrication of the RNA sequences biosensing platform

The manufacturer customizes Single-sided printed circuit boards. The PDMS prepolymer and the curing agent are first mixed and stirred evenly at a ratio of 15:1, then put in a vacuum drying oven and leave it for 15 min to remove air bubbles. Next, the prepolymer is poured on the stainless-steel plate (Hole diameter: 2 mm; Thickness: 1.65 mm). The electrode array is embedded in the prepolymer, which places it in an oven and cure at 60° for 8 h. Following cooling, take it out of the stainless-steel template to obtain the 4 × 4 mini-pillar array platform with the height of 1.65 mm and the diameter of 2 mm. Electrodes are then implanted in each mini-pillar to form a small electrochemical reactor so that silver nanostructure with different morphologies can be prepared to obtain the RNA sequences biosensing platform.

2.4. SERS detection of R6G and target sequences on the platform

A certain amount of Rhodamine 6G (R6G) powder was weighed with a precise analytical balance, and then a solution was prepared with ultrapure water to a concentration of 10^{-2} M. Finally, add water to dilute to different concentrations as needed (10^{-3} M–10^{-10} M) solution for backup. Take 2 μL of R6G solution and drop it on the SERS substrate that has been immobilized on the electrochemical platform with silver nanoparticles. After the reaction was left to dry at room temperature, use a Raman microscope with an excitation light source of 633 nm. Irradiation was performed to detect the SERS spectrum of R6G. The same approach applied to the target sequences detection. After 15 min of reaction with 2 μL target sample mixed with capture probe and detection probe, SERS detection was performed with 633 nm excitation laser source.

3. Results and discussion

3.1. Arrayed COVID-19 detection mini-pillar platform

Fig. 1 demonstrated the programmed nanomaterial synthesis and subsequent SARS-CoV-2 RNA sequences SERS detection. The whole processes for such platform mainly include mini-pillar-based platform fabrication, multiple nanomaterials regulation and characterization, and COVID-19 sampling and sensing. Briefly, we firstly prepared the basis of the whole platform using PDMS with 4 × 4 mini-pillars on top of the platform as shown in Fig. 1a, with three electrodes implanted in each mini-pillar (Ag as the working electrode, Ag/AgCl reference electrode, and Pt wire as the counter electrode) Each unit hold one droplet with quantitative composition and concentration of electrolyte solutions ($AgNO_3$/KNO_3 and sodium citrate/$AgNO_3$), which can achieve independently electrodeposition. The morphology of silver nanostructures could be controlled by adjusting the time and potential during electrodepositing. Finally, the appropriate nanostructures were selected for subsequently SERS sensing.

3.2. One-click optimization of mini-pillar sensing platform

Previous reports have confirmed that the morphology of Ag nanostructures can be affected by various parameters, such as electrodeposition time, potential, ambient temperature, and electrolyte composition [34–36]. And the preparation of silver nanoparticles by the electrodeposition method has good reproducibility [19,37]. Here we one-click investigated multiple silver nanostructures by integrated electrodeposition platform. Different silver nanostructures (dendritic, bulk, globular, and spiky) are formed by adjusting the corresponding parameters in array of 10 μL droplets as shown in Fig. 2. Firstly, we explored the effect of time and potential on the morphology of silver nanostructures.

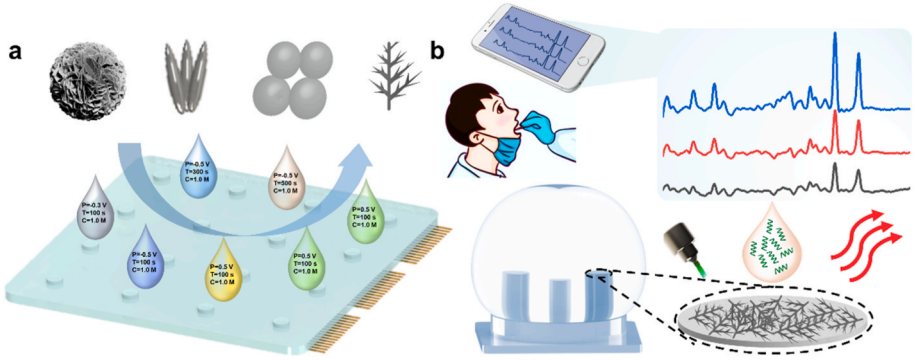

Fig. 1. Schematic illustration of mini-pillar-based chip for multiple silver nanostructures regulation and characterization (a), and for sensitive detection of COVID-19 biomarkers (b).

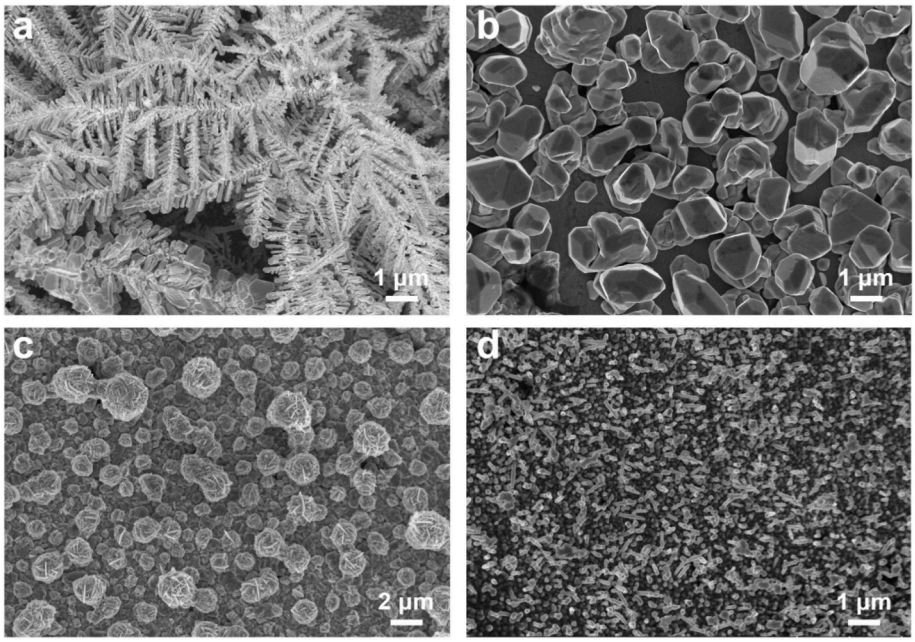

Fig. 2. SEM images of the resulting silver nanostructure at different electrochemical conditions. a) P: −0.5 V, T: 300 s, and C_{AgNO3}: 5 mg L^{-1}, b) P: −0.3 V, T: 300 s, and C_{AgNO3}: 5 mg L^{-1}, c) P: −0.3 V, T: 300 s, C_{AgNO3}: 5 mg L^{-1}, and $C_{sodium\ citrate}$: 5 mg L^{-1} d) P: −0.3 V, T: 300 s, C_{AgNO3}: 5 mg L^{-1}, and $C_{sodium\ citrate}$: 8 mg L^{-1} P: Potential T: Time.

At the potential (−0.5 V) and the $AgNO_3$ concentration is 5 mg L^{-1} promotes silver nanostructure's anisotropic differentiation to dendritic as shown in Fig. 2a and Figs. S1a–d. As shown in Fig. 2b and Figs. S1e–h, When the $AgNO_3$ concentration is 5 mg L^{-1} with the potential of −0.3 V, the obtained silver nanostructures are one by one bulk structure from 100 s to 800 s with negligible morphology change.

Notably, we investigated the composition of the electrolyte ($AgNO_3$/sodium citrate) in affecting morphology of Ag nanostructures as shown in Figs. S2a–d, At the 8 mg mL^{-1} of $AgNO_3$, the concentration of sodium citrate increased from 1 to 5 mg mL^{-1} (Potential: −0.3 V), the nanosheets with comparatively sharp edges gradually grew globular shape (Fig. 2c). Subsequently, when the concentration of sodium citrate was increased to 8 mg L^{-1}, the globular silver nanostructures gradually grew into a spiky shape (Fig. 2d), which was like a small wooden stick with the other end pointed. The silver nanostructure tended to be dendritic (Figs. S2e–h). Such results indicate that the electrolyte to $AgNO_3$ and sodium citrate could produce spherical and spiky shape silver nanostructures at the appropriate conditions. However, silver nanostructures still tended to dendrite with increasing sodium citrate concentration. Thus, we synthesized various morphologies of silver nanomaterials by regulating different parameters for subsequent detection.

Silver nanostructures with Raman enhanced properties have been widely applied in SERS sensing, and different morphologies directly affect the sensitivity and accuracy of detection [18,38,39]. We selected R6G as a model to verify that the Raman performance of bulk, dendritic, spiky, and globular substrates. The spectra of the SERS of R6G on a silver nanostructures SERS substrate in Fig. 3a showed that seven characteristic peaks at approximately 604, 764, 1173, 1304, 1355, 1506, and 1643 cm^{-1} were clearly observed as consistent with previously reported literature [40,41]. The dendritic silver nanostructures Raman signal was small at the R6G concentrations of 10^{-10} M, the Raman signal gradually increased as the R6G concentration increased (Fig. 3b). Raman signal intensity of such dendritic silver nanostructures was an order of magnitude higher than that of the other three morphological silver nanostructures (Fig. 3a). This should be attributed to a larger surface area and rougher nanostructure of the dendritic silver nanostructure than the other three nanostructures, which allows improving the detection efficiency and obtaining lowering the detection limit.

The overall trend of the bulk silver nanostructures Raman spectral signal increased continuously with the increasing R6G concentration as

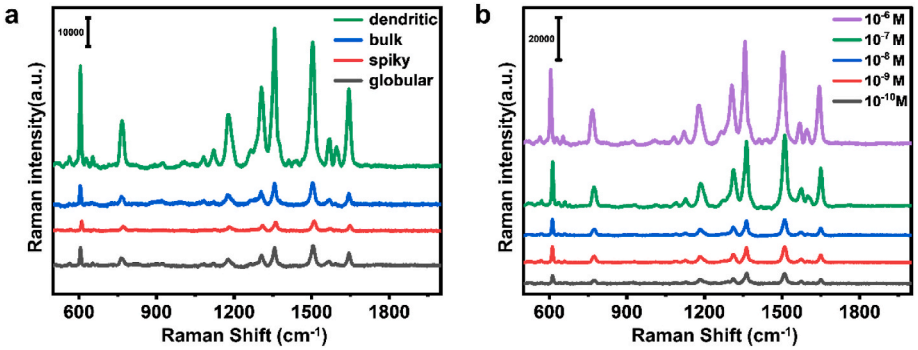

Fig. 3. Results of shape influence of silver nanostructures on Raman performance. a) SERS spectra of Bulk, dendritic, spiky and globular at the concentration of R6G at 10^{-3} M. b) SERS spectra of R6G microdroplets (from top: 10^{-6} M, 10^{-7} M, 10^{-8} M, 10^{-9} M and 10^{-10} M) on the silver dendritic nanostructures of substrate.

show in Fig. S3b. At a low concentration of R6G, the Raman signals of globular and spiky silver nanostructures are not very stable in the SERS spectrum of R6G and the Raman signal starts to gradually enhance from R6G concentration of 10^{-9} M to 10^{-6} M, which can be clearly observed from the figure. (Fig. S3c and Fig. S3d). This may be because the globular and spiky silver nanostructures were not well dispersed and stacked with each other to form high steric hindrance during the electrodeposition process, resulting in a reduced surface area that can accommodate fewer DNA probes. It was verified experimentally that these two morphologies were not suitable as substrates for SERS. Based on the above experiments, we found that the R6G signals of the dendritic silver nanostructures were more intense than those of the other three nanostructures because of their larger surface area and coarser nanostructures. Therefore, these results illustrate that the sliver nanostructures could be a good candidate for a sensitive SERS substrate.

3.3. Mini-pillar sensing platform for COVID-19 detection

Accurate detection of the COVID-19 allows early screening and diagnosis of coronavirus disease [42]. Fig. 4a illustrate the fabrication and sensing procedure of biosensor based on sandwich detection strategy. The DNA capture probe were firstly immobilized on the dendritic silver nanostructures surface. The presence of the target RNA sequence, the capture probe would immobilize the target RNA sequence along with

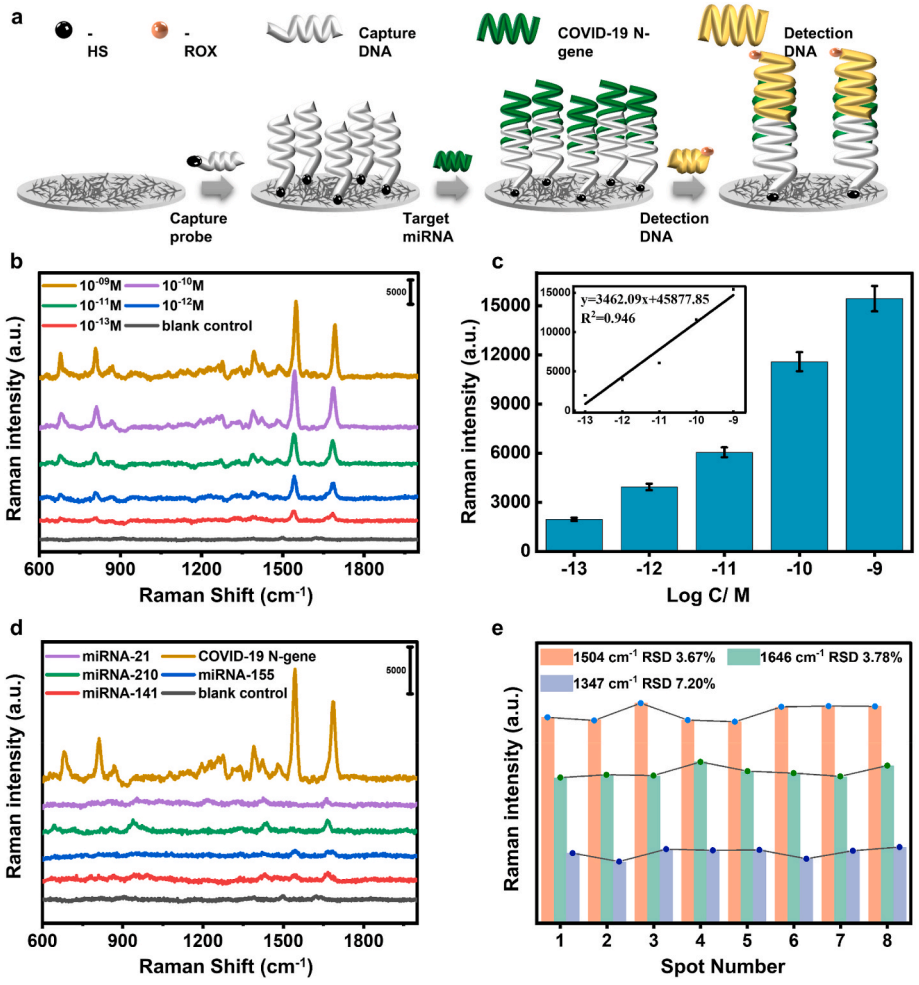

Fig. 4. Dendritic silver nanostructure for SARS-CoV-2 RNA sequence sensing. a) Illustration of detection process for SARS-CoV-2 RNA sequence. b) SERS spectra in the presence of SARS-CoV-2 RNA sequence with concentrations of 10^{-9}, 10^{-10}, 10^{-11}, 10^{-12} and 10^{-13} M, and blank control. c) Maximum peak value and linear (insets) relationship of SARS-CoV-2 RNA sequence in SERS spectrum. d) SERS spectra of miRNA-141, miRNA-155, miRNA-210, miRNA-21 and blank control. e) Intensity of the signal at 1504 cm^{-1}, 1646 cm^{-1} and 1347 cm^{-1} of 10^{-9} M ROX solution collected at eight array spots on the same base.

the detection probe on the chip. The sandwich structure could not be formed without target RNA due to surface limited capture probe hybridization, which prevents the Raman signal of Rhodamine X (ROX) molecule from being detected at the end of detection DNA as shown in Fig. S4a. Conversely, when detection DNA was added, a complete sandwich detection structure was formed, and the whole structure was fixed on the chip, the characteristic peak of ROX's Raman signal could be clearly seen.

We demonstrated the simultaneous detection of five concentrations of COVID-19 RNA sequence (10^{-9} to 10^{-13} M) by this strategy at room temperature with a 633 nm excitation laser source as shown in Fig. 4b. The specific Raman peak from the labeled probe on the detection DNA (635, 764, 1230, 1347, 1548, and 1646 cm^{-1}) was clearly observed and its peak information at 1548 cm^{-1} signal strength increases with concentration. The linear relationship between the Raman intensity and the logarithm of the target probe concentration is shown in Fig. 4c. It can be estimated from the figure that the limit of detection (LOD) of the technology is 7.42×10^{-14} M, and the linear range is 10^{-9} M–10^{-13} M. As shown in Fig. 4d, we also verified the specificity of the biosensing platform by replacing the SARS-CoV-2 RNA sequence with miRNA-141, miRNA-155, miRNA-210, miRNA-21, and blank control, and found that there was no significant change in signal intensity. To evaluate the platform's application in actual samples, we replaced the PBS buffer solution with human blood serum (Fig. S4b) for five concentrations of SARS-CoV-2 RNA sequences (10^{-9} to 10^{-13} M) sensing, as shown in Fig. S4b. We can also see that the Raman signal gradually increases with the increasing concentration of SARS-CoV-2 RNA sequences. Furthermore, reproducibility is a critical factor for SERS detection of trace biomarkers [43] (Fig. S5), and we examined the reproducibility of the dendritic silver nanostructures platform by taking eight different spots on the chip for SERS detection of ROX at a concentration of 10^{-9} M. Specific Raman signals of ROX molecules at 635, 764, 1230, 1347, 1548, and 1646 cm^{-1} were found for all eight sites, as shown in Fig. 4e, and we calculated the relative standard deviations (RSD) of 3.67%, 3.78% and 7.20% for the Raman signals at 1347, 1548 and 1646 cm^{-1}, respectively, and these experimental results indicate that The dendritic silver nanostructures biosensing platform for RNA sequence detection has good reproducibility for SERS detection of common and standard Raman molecular signals. The experimental results confirm that our platform has better performance than existing methods (Table S1), and has the potential to be further used for the detection of COVID-19 samples. Overall, we demonstrate the one-click biosensing platform has excellent reproducibility, stability, and specificity. Experimental results indicate that our biosensing chip has promising applications in biological sample detection species and has tremendous potential for accurate disease diagnosis.

4. Conclusion

In summary, we prepared multi-channel mini-pillar biosensor platform for the rapid, simple, and sensitive SERS detection of SARS-CoV-2 RNA sequence. We skillfully one-click synthesized four kinds of silver nanostructures with different morphologies by electrochemical deposition, which are bulk, dendritic, spherical, and spiny. Then, we screened the four morphologies of silver nanostructures by SERS. Dendritic silver nanostructures are the most effective enhanced Raman signals. The platform can detect multiple concentrations of SARS-CoV-2 RNA sequence simultaneously, thus significantly reducing the detection time and minimizing the influence of background signal and environment. This sensitive, well reproducible, low demand for samples, and specific biosensing platform can successfully detect multiple concentrations of SARS-CoV-2 RNA sequence with detection limits up to 7.42×10^{-14} M. The one-click investigation of shape influence of silver nanostructures on sensing performance has significant promise for disease prevention and control and precise disease detection.

CRediT authorship contribution statement

Zehua Li: contributed equally to this work, carried out the experiments, analyzed the data and wrote the manuscript. **Yong Luo:** contributed equally to this work, wrote and modified the manuscript. **Yongchao Song:** contributed equally to this work, carried out the experiments and analyzed the data. **Qinglin Zhu:** analyzed the data. **Tailin Xu:** supervised the project, modified the manuscript, and suppled the funding. **Xueji Zhang:** suppled the funding.

Declaration of competing interest

The authors declare that they have no known competing financial interests or personal relationships that could have appeared to influence the work reported in this paper.

Data availability

No data was used for the research described in the article.

Acknowledgments

We acknowledge funding from Shenzhen Stability Support Plan (20200806163622001), Joint Fund of the Ministry of Education for Equipment Pre-research (8091B0206), Shenzhen Overseas Talent Program, and Shenzhen Key Laboratory for Nano-Biosensing Technology (ZDSYS20210112161400001).

Appendix A. Supplementary data

Supplementary data to this article can be found online at https://doi.org/10.1016/j.aca.2022.340523.

References

[1] C. Dai, M. Guo, Y. Wu, B.P. Cao, X. Wang, Y. Wu, H. Kang, D. Kong, Z. Zhu, T. Ying, Y. Liu, D. Wei, J. Am. Chem. Soc. 143 (47) (2021) 19794–19801.
[2] C.M. Ackerman, C. Myhrvold, S.G. Thakku, C.A. Freije, H.C. Metsky, D.K. Yang, S. H. Ye, C.K. Boehm, T.F. Kosoko-Thoroddsen, J. Kehe, T.G. Nguyen, A. Carter, A. Kulesa, J.R. Barnes, V.G. Dugan, D.T. Hung, P.C. Blainey, P.C. Sabeti, Nature 582 (7811) (2020) 277–282.
[3] N.E. Sharpless, Science 368 (6497) (2020) 1290.
[4] L. Yao, W. Zhu, J. Shi, T. Xu, G. Qu, W. Zhou, X.F. Yu, X. Zhang, G. Jiang, Chem. Soc. Rev. 50 (6) (2021) 3656–3676.
[5] L.J. Carter, L.V. Garner, J.W. Smoot, Y. Li, Q. Zhou, C.J. Saveson, J.M. Sasso, A. C. Gregg, D.J. Soares, T.R. Beskid, S.R. Jervey, C. Liu, ACS Cent. Sci. 6 (5) (2020) 591–605.
[6] R.R.X. Lim, A. Bonanni, Trends Anal. Chem. 133 (2020), 116081.
[7] J. Zhang, S. Song, L. Zhang, L. Wang, H. Wu, D. Pan, C. Fan, J. Am. Chem. Soc. 128 (26) (2006) 8575–8580.
[8] J.M. Lee, H. Cho, Y. Jung, Angew. Chem. Int. Ed. 49 (46) (2010) 8662–8665.
[9] G. Seo, G. Lee, M.J. Kim, S.H. Baek, M. Choi, K.B. Ku, C.S. Lee, S. Jun, D. Park, H. G. Kim, S.J. Kim, J.O. Lee, B.T. Kim, E.C. Park, S.I. Kim, Rapid, ACS Nano 14 (4) (2020) 5135–5142.
[10] L.A. Lane, X. Qian, S. Nie, Chem. Rev. 115 (19) (2015) 10489–10529.
[11] C. Zong, M. Xu, L.J. Xu, T. Wei, X. Ma, X.S. Zheng, R. Hu, B. Ren, Chem. Rev. 118 (10) (2018) 4946–4980.
[12] M. Labib, E.H. Sargent, S.O. Kelley, Chem. Rev. 116 (16) (2016) 9001–9090.
[13] L. Zhu, X. Liu, J. Yang, Y. He, Y. Li, Anal. Chem. 92 (17) (2020) 11981–11986.
[14] J. Liu, X. Jiang, R. Zhang, Y. Zhang, L. Wu, W. Lu, J. Li, Y. Li, H. Zhang, Adv. Funct. Mater. 29 (6) (2018), 1807326.
[15] F. Le, D.W. Brandl, Y.A. Urzhumov, H. Wang, J. Kundu, N.J. Halas, J. Aizpurua, P. Nordlander, ACS Nano 2 (4) (2008) 707–718.
[16] X. Wu, X. Fan, Z. Yin, Y. Liu, J. Zhao, Z. Quan, Chem. Commun. 55 (55) (2019) 7982–7985.
[17] L. Ma, H. Wu, Y. Huang, S. Zou, J. Li, Z. Zhang, ACS Appl. Mater. 8 (40) (2016) 27162–27168.
[18] H.Y. Chen, M.H. Lin, C.Y. Wang, Y.M. Chang, S. Gwo, J. Am. Chem. Soc. 137 (42) (2015) 13698–13705.
[19] C. Zhu, G. Meng, P. Zheng, Q. Huang, Z. Li, X. Hu, X. Wang, Z. Huang, F. Li, N. Wu, Adv. Mater. 28 (24) (2016) 4871–4876.
[20] S.G. Park, C. Mun, M. Lee, T.Y. Jeon, H.S. Shim, Y.J. Lee, J.D. Kwon, C.S. Kim, D. H. Kim, Adv. Mater. 27 (29) (2015) 4290–4295.
[21] W. Yan, L. Yang, J. Chen, Y. Wu, P. Wang, Z. Li, Adv. Mater. 29 (36) (2017), 1702893.

[22] Z. Li, Y. Song, C. Fan, T. Xu, X. Zhang, Electroanalysis 33 (12) (2021) 2401–2405.
[23] S. Dick, M.P. Konrad, W.W. Lee, H. McCabe, J.N. McCracken, T.M. Rahman, A. Stewart, Y. Xu, S.E. Bell, Adv. Mater. 28 (27) (2016) 5705–5711.
[24] X. Song, T. Xu, Y. Song, X. He, D. Wang, C. Liu, X. Zhang, Talanta 218 (2020), 121206.
[25] E. Ben-Jacob, P. Garik, Nature 343 (6258) (1990) 523–530.
[26] J. Xi, Y. Ni, A. Liu, New J. Chem. 38 (4) (2014) 1738–1742.
[27] L. Xu, W. Yan, W. Ma, H. Kuang, X. Wu, L. Liu, Y. Zhao, L. Wang, C. Xu, Adv. Mater. 27 (10) (2015) 1706–1711.
[28] X. Qiao, X. Chen, C. Huang, A. Li, X. Li, Z. Lu, T. Wang, Angew. Chem. Int. Ed. 58 (46) (2019) 16523–16527.
[29] S.H. Sun, D.Q. Yang, D. Villers, G.X. Zhang, E. Sacher, J.P. Dodelet, Adv. Mater. 20 (3) (2008) 571–574.
[30] W. Jia, J. Li, G. Lin, L. Jiang, Cryst. Growth Des. 11 (9) (2011) 3822–3827.
[31] Y. Song, T. Xu, Q. Zhu, X. Zhang, Biosens. Bioelectron. 162 (2020), 112253.
[32] J. Xu, W. Gao, S. Jiang, Appl. Mater. Today 26 (2021), 101251.
[33] V.V. Nascimento, W.Q. Neves, R.S. Alencar, G. Li, C. Fu, R.C. Haddon, E. Bekyarova, J. Guo, S.S. Alexandre, R.W. Nunes, A.G. Souza Filho, C. Fantini, ACS Nano 15 (2021) 8574–8582.
[34] S.P. McDarby, C.J. Wang, M.E. King, M.L. Personick, J. Am. Chem. Soc. 142 (51) (2020) 21322–21335.
[35] G.C. Beaton, A.J. Bottomley, D. Prezgot, A. Ianoul, K.G. Stamplecoskie, J. Mater. Chem. C 8 (31) (2020) 10755–10760.
[36] Y.H. Chang, C. Liu, S. Rouvimov, T. Luo, S.P. Feng, Chem. Commun. 53 (50) (2017) 6752–6755.
[37] Y. Wang, L. Zhao, Y. Zhao, W.Y. Wang, Y. Liu, C. Gu, J. Li, G. Zhang, T.J. Huang, S. Yang, Adv. Mater. 30 (51) (2018), e1805686.
[38] D. He, B. Hu, Q.F. Yao, K. Wang, S.H. Yu, ACS Nano 3 (12) (2009) 3993–4002.
[39] P. Mohanty, I. Yoon, T. Kang, K. Seo, K.S. Varadwaj, W. Choi, Q.H. Park, J.P. Ahn, Y.D. Suh, H. Ihee, B. Kim, J. Am. Chem. Soc. 129 (31) (2007) 9576–9577.
[40] P. Hildebrandt, M. Stockburger, J. Phys. Chem. C 88 (24) (2002) 5935–5944.
[41] H.B. Li, P. Liu, Y. Liang, J. Xiao, G.W. Yang, Nanoscale 4 (16) (2012) 5082–5091.
[42] X. Dai, W. Fu, H. Chi, V.S.D. Mesias, H. Zhu, C.W. Leung, W. Liu, J. Huang, Nat. Commun. 12 (1) (2021) 1292.
[43] L. Shi, Z. Chu, Y. Liu, W. Jin, X. Chen, Biosens. Bioelectron. 49 (2013) 184–191.